An extracellular redox signal triggers calcium release and impacts the asexual development of *Toxoplasma gondii*

Eduardo Alves[1], Henry J. Benns[1,2], Lilian Magnus[1], Caia Dominicus[3], Tamás Dobai[1], Joshua Blight[1], Ceire J. Wincott[1], Matthew A. Child[1]*

[1]Department of Life Sciences, Imperial College London, Exhibition Road, South Kensington, London, SW7 2AZ, UK.

[2]Department of Chemistry, Imperial College London, Exhibition Road, South Kensington, London, SW7 2AZ, UK.

[3]Signaling in Apicomplexan Parasites Laboratory, The Francis Crick Institute, 1 Midland Road, NW1 1AT, London, UK

*To whom correspondence should be addressed: m.child@imperial.ac.uk

Abstract

The ability of an organism to sense and respond to environmental redox fluctuations relies on a signaling network that is incompletely understood in the apicomplexan parasite *Toxoplasma gondii*. The impact of changes in redox upon the development of this intracellular parasite is not known. Here, we provide a revised collection of 49 genes containing domains related to canonical antioxidant groups, with their encoded proteins widely dispersed throughout different cellular compartments. We demonstrate that addition of exogenous H_2O_2 to human fibroblasts infected with *T. gondii* triggers a Ca^{2+} flux in the cytosol of intracellular parasites that can induce egress. In line with existing models, egress triggered by exogenous H_2O_2 is reliant upon both Calcium-Dependent Protein Kinase 3 and diacylglycerol kinases. Finally, we show that the overexpression of the active catalytic domain of glutaredoxin in the parasitophorous vacuole severely impacts parasite replication. These data shed light on the rich redox network that exists in *T. gondii*, evidencing a link between extracellular redox and intracellular Ca^{2+} signaling that can culminate in parasite egress. Our findings also indicate that the redox potential of the intracellular environment contributes to normal parasite growth. Combined, our findings highlight the important role of redox as an unexplored regulator of parasite biology.

57 **Introduction**

58 *Toxoplasma gondii* is a single-cell obligate intracellular parasite from the apicomplexan phylum that
59 can infect any warm-blooded animal. Its seroprevalence is estimated at more than one-third of the
60 human population [1, 2]. Within the host, the asexual lifecycle of *T. gondii* exists as two distinct stages:
61 rapidly proliferating tachyzoites that characterize the acute infection, and slower replicating encysted
62 bradyzoites that are associated with chronic infection[3, 4]. While infections are usually benign, in
63 immunocompromised patients and foetuses[5, 6] the lytic tachyzoite lifecycle is responsible for severe
64 clinical pathology. During a lytic cycle, tachyzoites attach onto and actively penetrate host cells,
65 forming a permissive replication niche called the parasitophorous vacuole (PV). Parasites then
66 replicate by endodyogeny[7] until they eventually egress from the host cell, leading to its lytic
67 destruction. The interconversion of virulent tachyzoites with persistent encysted bradyzoites is
68 influenced by host immune pressure and is key to understanding disease recrudescence[8]. The ability
69 of *T. gondii* to infect diverse host species is related to its remarkable capacity to resist host defences.
70 Moreover, it must be able to efficiently recognize and quickly respond to a myriad of environmental
71 clues. Among biological signal cascades activated by external clues, Ca^{2+} signaling is the most notable
72 and best studied in *Toxoplasma* (reviewed in [9]). Ca^{2+} is a ubiquitous signaling molecule with a vital
73 role in tachyzoite host-cell invasion[10, 11], motility[12] and egress[13] through activation of effector
74 proteins such as the plant like Ca^{2+}-dependent Protein Kinase 1 (CDPK1)[14, 15] and CDPK3[16].
75 Alongside Ca^{2+}, other intracellular signaling molecules are known to play important roles in the
76 tachyzoite lytic cycle. These include phosphatidic acid (PA)[17], and the activation of protein kinase G
77 by cyclic guanidine monophosphate (cGMP)[18].

78 Contrasting with Ca^{2+}, the study of reactive oxygen species (ROS) as signaling molecules is
79 incipient in the Apicomplexa. Hydrogen peroxide (H_2O_2) is a neutral ROS molecule with an ability to
80 cross membranes[19], and its roles in signaling are diverse. These include its interaction with
81 glutathione (GSH), and the oxidation of cysteine residues leading to allosteric changes in a variety of
82 proteins such as phosphatases, transcription factors and ion channels[20]. Typically, the oxidation of
83 redox-sensitive cysteines is a reversible process catalysed by enzymes that use GSH or nicotinamide
84 adenine dinucleotide phosphatase (NADPH)[21-24] as redox cofactors. Most studies of H_2O_2 and *T.*

85 *gondii* tachyzoites have focused on the ability of host cells to use the damaging oxidative properties of
86 ROS as a component of innate defence, and strategies employed by tachyzoites to overcome this
87 defence[25-29].

88 A *T. gondii* orthologue of the H_2O_2-detoxifying enzyme catalase is expressed in the parasite
89 cytosol, and confers protection against host oxidative stress[26, 30]. In 2004 Ding *et al.,* [26] compiled a
90 group of 14 genes related to the *T. gondii* antioxidant system. These typically localized to the parasite
91 cytosol and mitochondria, and were assigned to one of five major redox system classifications: (1)
92 metabolic genes (e.g. superoxide-dismutase and catalase); (2) thioredoxins (proteins that promote
93 cysteine thiol-disulfide exchange); (3) Protein Disulfide Isomerases (PDIs, proteins that disrupt or
94 form cysteine disulfide bonds to assist protein folding); (4) glutaredoxin-glutathione (Grx-GSH, small
95 proteins that use GSH as a cofactor for thiol-disulfide exchange) and (5) peroxiredoxins (Prxs,
96 enzymes that detoxify hydroperoxides like H_2O_2 and organic hydroperoxides).

97 Expanding this broad description of the parasite's antioxidant system, other studies have
98 tested the association of redox with *T. gondii* signaling and cell cycle regulation. Exogenous treatment
99 of intracellular parasites with the reducing agent dithiothreitol (DTT) triggers Ca^{2+} mobilization and
100 parasite egress[31]. This egress was triggered by host-cell ATP depletion resulting from the activity of
101 an exported parasite ATPase[32]. In a separate study, the oxidation-sensitive protein *Tg*DJ-1 was found
102 to associate with CDPK1 and promote microneme secretion in *Toxoplasma*[33]. More recently,
103 oxidative stress (generated by sodium arsenite) has been shown to trigger tachyzoite differentiation
104 into bradyzoites following phosphorylation of *Toxoplasma* translation initiation factor kinase
105 (*Tg*IF2K-B)[34]. Together, these data suggest that *T. gondii* modulates various biological processes in
106 response to changes in both the reduction and oxidation status of the environment.

107 In this study, we begin by revisiting existing datasets to identify genes related to redox
108 systems and update our view of these genes in *T. gondii*. We then investigate the impact of H_2O_2 upon
109 parasite biology, demonstrating that an H_2O_2 signal outside the boundaries of the infected host cell can
110 be received and interpreted deep within the cytosol of intracellular parasites. Extracellular H_2O_2
111 triggers mobilization of Ca^{2+} culminating in CDPK3-dependent egress. Finally, we use a genetically
112 encoded redox reporter to dissect redox oscillations prior to egress. Unexpectedly, we discover that

113 overexpression of the active catalytic domain of a human glutaredoxin enzyme in the parasite's
114 cytosol or PV delays parasite asexual replication. Our results corroborate the existence of a rich
115 variety of antioxidant proteins located in multiples cellular compartments, and highlight importance
116 of redox in the basic biology of *Toxoplasma*.
117
118 **Results**
119 *Updated T. gondii redox-associated genes and their primary predicted protein localisation*
120 We initially sought to update our understanding of the antioxidant response and redox-signaling
121 network in *T. gondii*. We mined gene sequence and annotation information, as well as proteomic
122 datasets present on ToxoDB to update the list of 14 redox associated genes previously summarised
123 and reported by Ding *et al.,* 2004[26]. Our bioinformatic approach screened for genes containing at
124 least one functional domain of the major redox signaling groups (Trxs, PDIs, Grx-GSHs and Prxs).
125 We identified a total of 49 redox-associated genes (Supplemental material table S1), including 20
126 Trxs, 13 GRX-GSHs, six PDIs, six Prxs, and four metabolic genes (including three distinct
127 superoxide dismutases and one catalase). With the exception of the metabolic genes that have been
128 more thoroughly investigated[26, 30, 35, 36], most genes representing the other redox signaling groups
129 remain uncharacterized. For an improved view of the subcellular distribution of these gene products,
130 we extracted their primary localisation from the recently published hyperLOPIT dataset[37] (Figure 1 –
131 table supplement 1). This indicated a broad distribution of these proteins throughout the cell, and
132 suggested the existence of spatially distinct mechanisms of redox regulation for different subcellular
133 compartments.

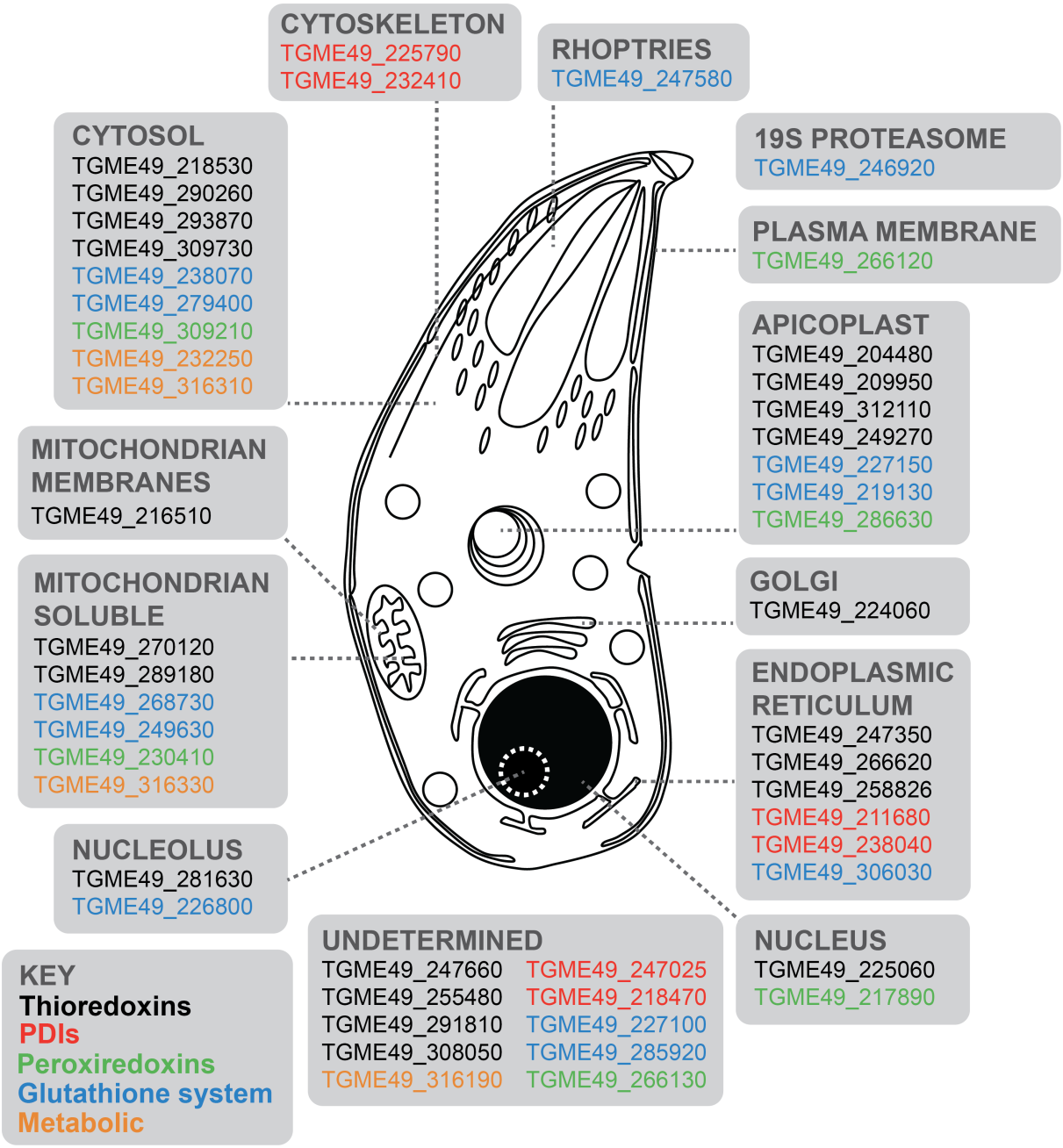

Figure 1: Schematic representation of a *T. gondii* tachyzoite displaying 49 redox-associated genes and their primary HyperLOPIT[37] protein location. Gene ID accession numbers are provided, and genes categorized into five groups: black (Trxs); red (PDIs); green (Prxs); blue (Gxr-GHSs) and orange (metabolic genes). Further details are provided in Supplement table S1.

144 *Extracellular hydrogen peroxide induces cytosolic Ca^{2+} flux in intracellular tachyzoites*

145 In other eukaryotic systems there is an association between calcium and redox signaling. For example,
146 oxidation of the ryanodine receptor is known to stimulate calcium release from intracellular
147 compartments[38, 39]. To investigate if a similar overlap exists between these two signaling networks in
148 *Toxoplasma*, we tested the ability of H_2O_2 to trigger a Ca^{2+} response in tachyzoites within a host cell.
149 We generated a Type 1 parasite (RH strain) expressing the Ca^{2+} sensor protein jRCamP1b[40] fused
150 with GFP (referred to as RH-GFP-2ta-jRCamP1tb). The ratio of these two distinct fluorescent
151 proteins provided an elegant tool to distinguish changes in fluorescence due to parasite movement
152 from the Ca^{2+} signal (Figure 2 – figure supplement 1A). Upon exogenous addition of 100 μM H_2O_2
153 we observed a distinct spike in the intracellular Ca^{2+} reporter signal (Figure 2A). To determine
154 whether the oxidative properties of H_2O_2 are responsible for triggering parasite Ca^{2+} release, we
155 repeated the experiment in the presence of the antioxidant α-tocopherol (Figure 2B). Pre-treatment of
156 infected host cell monolayers with 50 μM α-tocopherol abolished H_2O_2-stimulated Ca^{2+} release in
157 intracellular parasites. The addition of the Ca^{2+} ionophore A23187 caused an intense Ca^{2+} signal spike
158 in the parasite cytosol in both the presence and absence α-tocopherol (Figure 2A and 2B, respectively),
159 suggesting that the presence of the antioxidant does not interfere with Ca^{2+} stores in intracellular
160 parasites. Vehicle solvent for H_2O_2 (water) and for A231877 (DMSO) did not trigger Ca^{2+}
161 mobilisation (Figure 2 – figure supplement 1B and 1C, respectively).

162 To have a reference for the intensity of the Ca^{2+} signal spike induced by H_2O_2, we compared the Ca^{2+}
163 signal increase over the resting baseline against A23187 (Figure 2C), a small molecule known to
164 induce parasite egress by Ca^{2+} dependent mechanisms[41]. H_2O_2 induced an overall Ca^{2+} signal
165 increase of 35% ± 1.7. This was lower than the Ca^{2+} signal increase observed when parasites were
166 treated with A23187 alone (140 ± 4.3), or A23187 on cells pretreated with 100 μM H_2O_2 (61% ± 0.9).
167 Accordingly, within the 10 minutes tracking the parasites, only one event of egress was observed for
168 cells treated with 100 μM H_2O_2. We also compared the intensity of Ca^{2+} signal increase induced by
169 H_2O_2 with Δ*CDPK3* line (Figure 2D). The intensity of the Ca^{2+} signal induced by H_2O_2 on RH-GFP-
170 2ta-jRCamP1bΔ*CDPK3* was lower (18.1% ± 4.3) compared to RH-GFP-2ta-jRCamP1b (32.5% ± 1.1).
171 This could reflect previously observed differences in the resting Ca^{2+} levels of these lines[42]. These

172 data suggest that tachyzoites within the PV can perceive and respond to oxidation events outside the
173 host cells.
174
175 *Hydrogen peroxide induces parasite egress in a mechanism dependent on CDPK3*
176 Calcium flux accompanies natural egress[43], and calcium ionophores are well-characterized inducers
177 of egress[13]. To better investigate the potential of H_2O_2 to induce parasite egress, we analysed
178 populations of infected host cells by flow cytometry. We used the GFP signal from parasites
179 expressing the Ca^{2+} sensor and particle size to distinguish infected host cells from free tachyzoites
180 (Figure 2 – figure supplement 2A). We tested whether a longer treatment (30 mins) with different
181 concentrations of H_2O_2 could increase the number of free tachyzoites. Incubation of infected host cells
182 with H_2O_2 resulted in a dose-dependent increase in the number of free tachyzoites (Figure 2E). We
183 sought to understand how the H_2O_2 stimulated egress integrates into the existing molecular model of
184 egress. The small molecule R59022 is an inhibitor of diacylglycerol kinase[44] that has been shown to
185 inhibit egress by affecting the formation of phosphatidic acid[17]. H_2O_2 treatment resulted in a partial
186 pharmacological rescue of R59022 egress inhibition. This partial rescue could relate to the discrete
187 points of activity for the two targets of R59022: diacylglycerol kinase 1 and 2[45]. The stimulation of
188 egress by H_2O_2 was abolished in Δ*CDPK3* parasites (Figure 2F), demonstrating a dependency upon
189 this kinase similar to other egress agonists such as A231287. The incubation of non-infected HFFs
190 with different concentration of H_2O_2 did not alter the proportion of events in this population (Figure 2
191 – figure supplement 2B) confirming that the concentrations of H_2O_2 used in this protocol did not lysed
192 the host cells.
193
194

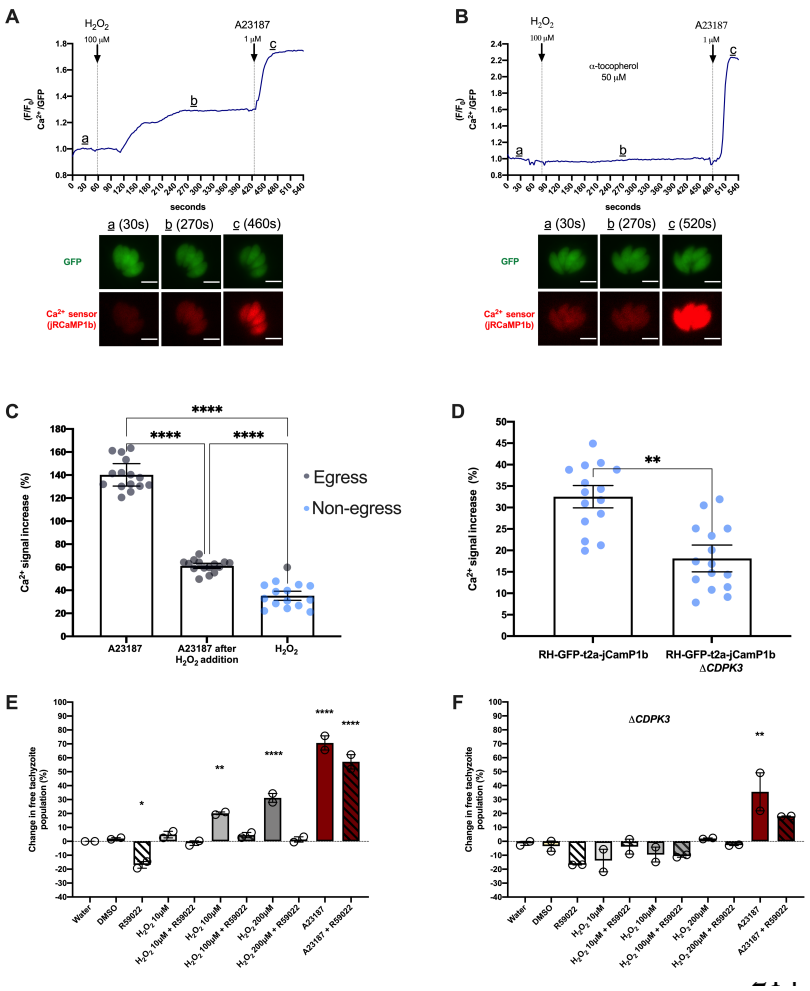

Figure 2: H_2O_2 induces Ca^{2+} release in intracellular parasites and triggers CDPK3-dependent egress. (**A**) Representative trace of H_2O_2 induction of Ca^{2+} flux in intracellular RH-GFP-2ta-jRCamP1b parasites, followed by A23187 treatment. a – c: widefield microscopy images depicting changes in parasite fluorescence signal intensity for both GFP and the Ca^{2+} sensor at baseline (a at 30s), the peak of Ca^{2+} after H_2O_2 addition (b at 270s), and peak of Ca^{2+} after A23187 addition (c at 460s). Data are representative of 27 infected vacuoles from four independent experiments. (**B**) Representative trace of H_2O_2 induction of Ca^{2+} flux following pre-treatment of infected host cells with 50 µM α-tocopherol. a: baseline at 30s, b: trace after H_2O_2 addition at 270s and c: peak of Ca^{2+} triggered by A23187 at 520s. Data are representative of 14 infected vacuoles from three independent experiments. For (**A**) and (**B**): black arrows indicate the time of compound addition. Scale bar: 5 µM. (**C**) Intensity of parasite Ca^{2+} signal increase in RH-GFP-2ta-jRCamP1b parasites (expressed as a percentage over baseline) following addition of: 1 µM A23187, 1 µM of A23187 after 100 µM H_2O_2 treatment, and 100 µM H_2O_2 alone. Gray dots indicate vacuole data points where parasite egress was observed during the measurement timeframe, blue dots represent vacuoles where egress was not observed. (**D**) Intensity of parasite Ca^{2+} signal increase (%) over the baseline upon addition of 100 µM H_2O_2 in RH-GFP-2ta-jRCamP1b versus RH-GFP-2ta-jRCamP1bΔ*CDPK3* parasites. For (**C**) and (**D**): histograms present data mean ±SEM of three independent experiments (five vacuoles measured in each experiment), with individual vacuole data points also shown. (**E**) and (**F**): Egress assay measuring tachyzoite release after compound treatment in RH-GFP-2ta-jRCamP1b and RH-GFP-2ta-jRCamP1bΔ*CDPK3*, respectively. Data represent the mean ±SEM of two independent experiments, with six technical replicates for each. All data were normalised to the water control. Significance was calculated using one-way Anova, Bonferroni's multiple comparisons test. P values: *< 0.05; **< 0.01 and ****< 0.0001.

232 *Intracellular parasites expressing GRX1-roGFP2 sensor perceive oxidation induced by H_2O_2*

233 After confirming that exogenous addition of H_2O_2 stimulated Ca^{2+} flux in intracellular *Toxoplasma*
234 parasites, we investigated the redox state within the parasite cytosol and PV during process. We
235 reasoned that if calcium release was the direct result of an oxidative signal, that the redox status of
236 cellular compartments separating intracellular parasites from the extracellular environment should
237 also be affected. To test this, we generated transgenic parasite strains constitutively expressing the
238 redox sensor protein GRX1-roGFP2, in two different cellular compartments: the parasite cytosol, or
239 targeted to the PV as a consequence of an N-terminal fusion with the GRA8 signal sequence[46].
240 GRX1-roGFP2 is a ratiometric redox reporter that detects changes in both reduced (GSH) and
241 oxidized (GSSG) glutathione[47] (Figure 3A). GRX1-roGFP2 is a sensitive tool to measure rapid
242 changes in GSH/GSSG. Importantly, the redox relay system underpinning GRX1-roGFP2 is not
243 affected by pH, which is known to confound data interpretation with other redox sensor proteins[48].
244 We used GRX1-roGFP2 parasites to track dynamic changes in GSH/GSSG by fluorescence
245 microscopy, and used the normalized GSH/GSSG signal ratio to measure the intensity of oxidation
246 events (Figure 3B – figure supplement 3A). Intracellular parasites expressing the redox sensor
247 targeted to the PV (RH-GRA8-GRX1-roGFP2) or cytosol (RH-GRX1-roGFP2) both confirmed an
248 oxidation event upon exogenous addition of 100 μM H_2O_2 (Figure 3C and D, respectively). The
249 oxidation event was of a greater magnitude within PV compared to that detected within the parasite
250 cytosol, indicating the anticipated decrease in the strength of the oxidation signal as it crossed the
251 biological membrane separating these compartments. The water control did not affect the redox signal
252 from GRX-roGFP2 sensor (Figure 3 – figure supplement 3B).

253 Having observed that H_2O_2 could stimulate calcium flux, we investigated the reciprocal
254 nature this relationship, testing the ability of calcium ionophores to trigger an oxidative event. Using
255 GRX1-roGFP2 parasites, we measure the resting redox state prior to ionomycin-induced egress.
256 Ionomycin-induced egress was not accompanied by detectable changes in redox within either the PV
257 or parasite cytosol (Figure 3E and F, respectively). The ionophore A23187 could not be used because
258 of saturating autofluorescence associated with this small molecule in the fluorescence channel used to

measure oxidation (Figure 3 – figure supplemental 3C). These data suggest that no significant change in the GSH/GSSG ratio occurs before parasite egress.

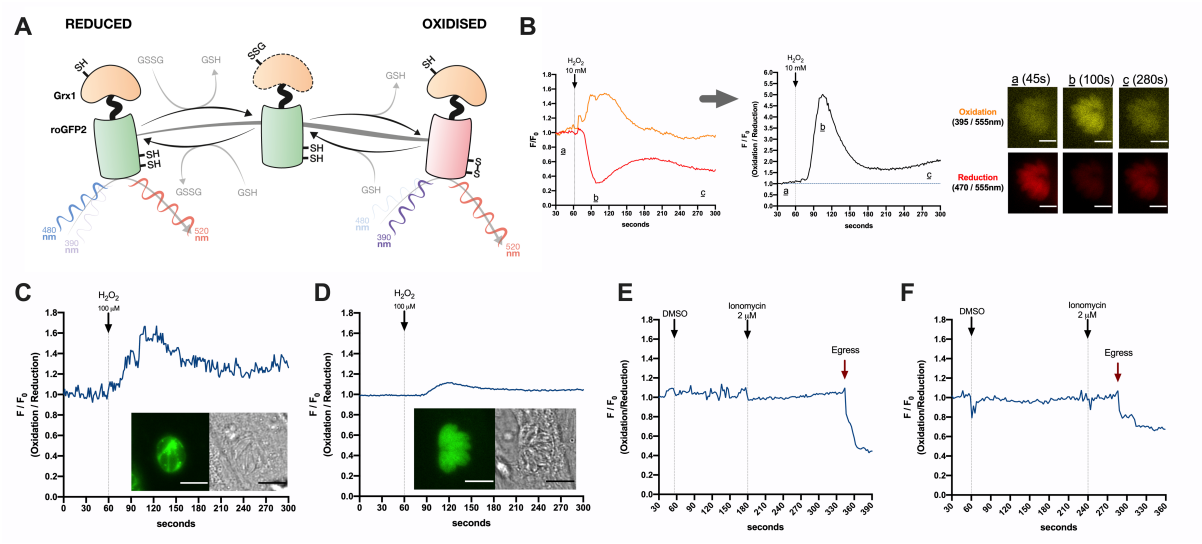

Figure 3: Oxidation induced by exogenous H_2O_2 results in a redox change within the PV and parasite cytosol. (**A**) Schematic representation of the redox sensor based on the catalytic domain of glutaredoxin (Grx1) fused with ro-GFP2 depicting how this sensor interacts with GSH/GSSG and the excitation and emission values of the reduced and oxidised states. (**B**) Proof-of-principle tracking dynamic changes of GSH/GSSG during an oxidation event in RH-GRX1-roGFP2 parasites. The left graph panel presents a representative signal trace from the GRX1-roGFP2 sensor monitoring both fluorescence channels for reduced (red line) and oxidized (orange line) readouts over time. The right graph panel presents the oxidation/reduction ratio of normalized signal depicting the intensity changes in redox compared to baseline. Microscopy images of an infected vacuole presented in pseudocolor (orange for oxidation, red for reduction) at a: baseline (45s), b: at the peak of the oxidation event (100s) and c: the return to baseline (280s). This is a representative trace from two independent experiments, with eight vacuoles. (**C**) Representative trace from RH-GRA8-GRX1-roGFP2 parasites depicting H_2O_2 induced redox change within the PV. Microscopy images of an infected vacuole highlighting the presence of the sensor within PV (left image), alongside the brightfield image of the infected host cell. (**D**) A representative trace from RH-GRX1-roGFP2 parasites depicting H_2O_2 induction of redox change within the parasite cytosol. Microscopy images depicting an infected vacuole highlighting the presence of the sensor on cytosol (left panel image) alongside the brightfield image of the infected host cell. (**C – D**): Representative traces from three independent experiment, nine vacuoles for each group. (**E** and **F**): Representative trace of redox fluctuations in intracellular parasite following ionomycin treatment for RH-GRA8-GRX1-roGFP2 (**E**), and RH-GRX1-roGFP2 parasites (**F**). (**E – D**): red arrows indicate the moment of parasite egress. Representative traces from three independent experiments, nine vacuoles for each group.

313 *GRX1-roGFP2 redox sensor affects parasite fitness during asexual replication*

314 We noted that one unavoidable result of using the GRX1-roGFP2 redox relay sensors would be the
315 associated overexpression of the catalytic domain of glutaredoxin (as a consequence of it being fused
316 to roGFP2). GRX1 is a small redox enzyme that confers protection against oxidative stress[48, 49], and
317 the overexpression of this enzyme would be expected to shift GSH/GSSG ratios in favour of the
318 reduced form (GSH). Correspondingly, we hypothesized that *Toxoplasma* parasites overexpressing
319 GRX1 would have their normal redox status shifted to a more reduced potential. To test whether the
320 overexpression of this redox protein affected parasite asexual growth, we generated a transgenic
321 parasite strain expressing a version of the redox sensor where we had mutated the key catalytic
322 residue of GRX to render it enzymatically inactive ($GRX1_{ser}$-roGFP2). As a result, GRX1ser-roGFP2
323 sensor did not respond changes in GSH/GSSG following H_2O_2 treatment (Figure 4 - figure
324 supplement 4). We compared the growth of this strain with parasites expressing the catalytically
325 active version of the sensor. As before, both active and inactive versions of the GRX-fusion sensor
326 were targeted to either the parasite cytosol or PV. As a control group, we used a parasite strain
327 expressing redox-insensitive GFP (RH-GFP-Luc). Parasites expressing catalytically active GRX1 in
328 the cytosol presented fewer plaques compared to RH-GFP-Luc (Figure 4A). Despite being able to
329 successfully maintain PV-targeted sensor strains in culture, all parasites lines where the sensor was
330 targeted to the PV did not form clear measurable plaques after six days of growth. Intensely stained
331 plaque-shaped boundaries visible on the HFF monolayer suggested these parasites had successfully
332 grown, but that parasite lytic growth had not outcompeted host cell monolayer recovery sufficiently to
333 produce a clear zone of lysis (Figure 4B). When either the catalytically active or inactive sensors were
334 targeted to the parasite cytosol, parasites formed smaller plaques compared to the RH-GFP-Luc
335 control (Figure 4B and 4C, respectively). These data suggested that the presence roGFP2 alone might
336 be sufficient to affect parasite growth. To directly test the influence of redox environment on the lytic
337 cycle, we grew RH-GFP-Luc parasites with 10 μM N-acetyl cysteine (NAC), a small antioxidant
338 molecule that functions by donating cysteine to increase GSH biosynthesis[50]. Addition of NAC
339 decreased the size of plaques generated by RH-GFP-Luc parasites (Figure 4C), suggesting that
340 GSH/GSSG imbalance compromised parasite growth. To better understand the impact of

overexpressing the sensor on parasite growth, we counted the number of parasites per vacuole after 20 hours of asexual parasite replication (Figure 4D). All strains expressing the redox sensor had reduced replication compared to RH-GFP-Luc (Figure 4 – figure supplement 5), with catalytic inactivation of the GRX domain providing a partial rescue of the replication defect. Strains exhibiting the slowest replication were those where the sensor was targeted to the PV, supporting the plaque growth data in Figure 4B. Altogether, these data suggest that shift in GSH/GSSG buffer system, in either the parasite cytosol or the PV slows parasite growth.

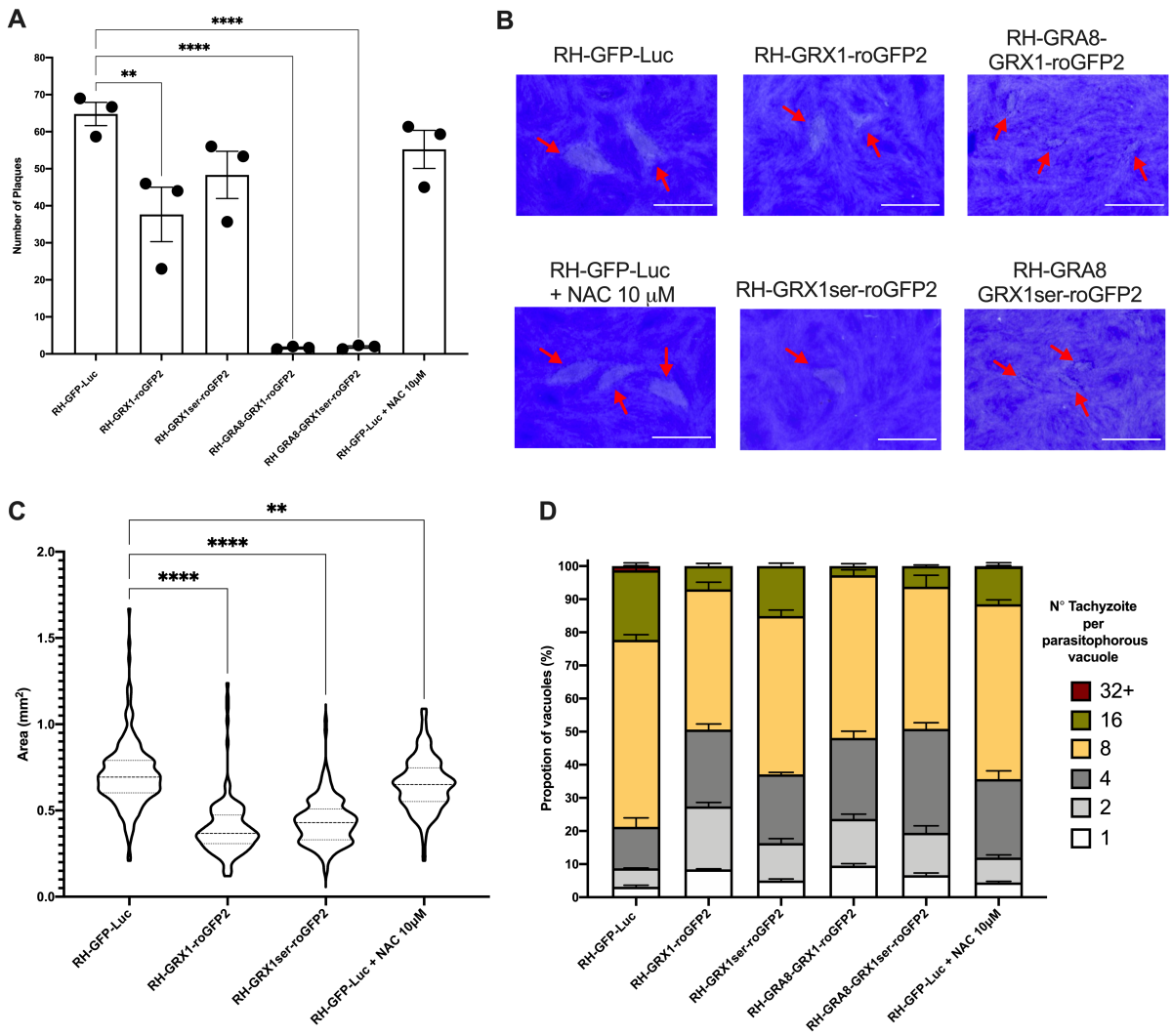

Figure 4: The GRX1-roGFP redox sensor affects parasites fitness during asexual replication. (**A**) Histogram presenting plaque count data from a 6-day plaque assay using RH-GFP-Luc parasites as a reference control group. (**B**) Representative images of plaques formed. Plaques are indicated by red arrows. Scale bar: 2 mm. (**C**) Violin plot presenting the distribution of plaque areas (mm^2) for parasites expressing the redox sensor within the cytosol. (**D**) Histogram presenting the effect of the GRX1-roGFP sensors and NAC on parasite intracellular replication. (**A** – **D**) All obtained from three independent experiments, with three technical replicates. Significance was calculated using one-way Anova, Bonferroni's multiple comparisons test for (**A**) and (**B**). P values: **< 0.01, **< 0.001 and ****< 0.0001. The significance analyse for (**D**) is provide on figure supplement 5.

383 **Discussion**

384 Investigations of ROS molecules like H_2O_2 and *T. gondii* initially focused on the host innate immune
385 response. Host macrophage can generate oxidative bursts, creating a toxic microenvironment to fight
386 microbial infection[51-53], with early studies interested in mechanisms used by *Toxoplasma* to evade
387 oxidative stress[54-56]. However, increasing evidence from multiple organisms has demonstrated that
388 H_2O_2 has functions as a signaling molecule (reviewed in [57]), suggesting the likelihood of a more
389 complex role for ROS in the pathophysiology of *Toxoplasma*. In order to sense, respond, and protect
390 against potential oxidative damage from a ROS stimulus, cells employ a network of redox-associated
391 proteins like thioredoxins, PDIs, Prxs, superoxide dismutase, catalase and Grx-GSH. It was
392 previously shown that *Toxoplasma* possesses all these elements[26], and we provide an updated view of
393 the number, diversity and cellular distribution of these redox-associated proteins (Fig.1). The function
394 of some of these redox-associated gene products in *T. gondii* parasites has been examined: disruption
395 of catalase decreases parasite virulence in mice and *in vitro* tolerance to H_2O_2 [26]; peroxiredoxin-1
396 interacts with histone lysine methyltransferase to likely regulate genes by chromatin rearrangement[58];
397 two thioredoxins mediate an essential role in apicoplast biogenesis[59], and another thioredoxin with
398 cytosolic localization has been associated with parasite virulence[60]. Nevertheless, functional
399 information for most of the redox-associated proteins identified in this work remains elusive.

400 The ability of low concentrations of H_2O_2 to initiate an intracellular Ca^{2+} response in mammal
401 models is well documented in the literature[61-63] and helped to solidify H_2O_2 as a signaling molecule.
402 Addition of antioxidants blocks intracellular Ca^{2+} release induced by H_2O_2 in smooth muscle cells[63]
403 suggesting that the oxidative properties of H_2O_2 are required for Ca^{2+} signaling. In human endothelial
404 cells, oxidation induced by non-toxic concentrations of H_2O_2 target a Ca^{2+} channel located in acid
405 compartments[62]. Distinct from these models, this work is the first to report that an oxidation event
406 induced by H_2O_2 mobilizes intracellular Ca^{2+} in *Toxoplasma* parasites within the infected host cell
407 (Fig. 2A). Studying the parasite within the host cell provides the best approximation of physiological
408 conditions to observe both Ca^{2+} and redox signaling. Moreover, using parasites expressing a
409 genetically encoded fluorescent Ca^{2+} sensor abrogated the need to use fluorescent Ca^{2+} indicator dyes.
410 Use of these dyes can be damaging to the cells, and typically require the use of other small molecules

411 to avoid dye loss and compartmentalization[64]. GFP co-expressed with Ca^{2+} sensor allows Ca^{2+}
412 responses to be distinguished from parasite movement which avoids the need to use inhibitors of
413 parasite motility such as cytochalasin D[65]. Finally, the concentration of 100 μM H_2O_2 has been
414 showed to be non-toxic for human fibroblast[66]. Altogether, our protocol to investigate intracellular
415 Ca^{2+} release following H_2O_2 treatment sought to avoid cellular stress that could compromise the true
416 redox/Ca^{2+} dynamic within the parasite. As previously report in muscle cells[63], the presence of
417 antioxidant inhibited the parasite Ca^{2+} response triggered by H_2O_2. Using the GRX1-roGFP2 redox
418 sensor, we confirmed that intracellular parasites directly sense an oxidation event following the
419 exogenous addition of 100 μM H_2O_2. It is not clear whether the exogenous addition of 100 μM of
420 H_2O_2 results in H_2O_2 reaching the intracellular parasites as the host cell contains an extensive network
421 of antioxidant proteins that would be expected to scavenge and neutralise H_2O_2. This could be directly
422 addressed in future experiments using *Toxoplasma* parasites expressing a sensor that specifically
423 detects H_2O_2[67].

424 Regardless of whether Ca^{2+} is mobilized within the parasite as a direct result of an interaction
425 with H_2O_2, or via secondary oxidation signal from the host, Ca^{2+} regulates all aspects of parasite host
426 cell invasion[9] included egress[16]. For the short time period used to track parasites by microscopy, the
427 intensity of the Ca^{2+} signal spike induced by H_2O_2 was quite modest compared to A23187, and that
428 likely explains why egress events were rare. Longer incubations with H_2O_2 induced parasite egress
429 through a mechanism that requires CDPK3 and likely phosphatidic acid. This is the first evidence that
430 suggests that oxidation can trigger egress in *Toxoplasma.* Interestingly, at the other end of the redox
431 spectrum, the reductive molecule DDT can also mobilize Ca^{2+} and induce parasite egress[31].
432 Although the mechanism by which H_2O_2 and DDT lead to parasite egress appears to be distinct, these
433 data indicate that redox can influence the parasite's lytic cycle. We anticipate that parasite biology is
434 tuned to a specific environmental redox potential, and that the perturbation of redox homeostasis with
435 either oxidative or reductive stress elicits a phenotypic response.

436 The mechanism for how H_2O_2 mobilizes Ca^{2+} in animals is better understood but the
437 evolutionary distance between vertebrates and *Toxoplasma* makes direct comparisons uninformative.
438 *Toxoplasma* is more closely related to plants and share a more similar signaling toolkit[68]. It has been

439 recently reported that plants possess a cell surface H_2O_2 receptor that once activated, triggers a Ca^{2+}
440 influx into the cells through a Ca^{2+} ion channel[69]. *Toxoplasma* also has a H_2O_2-sensitive protein that
441 associates with the CDPK1 to promote microneme secretion[33], an event that requires Ca^{2+}
442 mobilization to allow parasite invasion[70].

443 Our work suggests a connection between oxidation and parasite Ca^{2+} release but our data did
444 not find evidence that ionophore-induced Ca^{2+} release changes the redox state of either the parasite's
445 cytosol or PV. The use of the GRX1-roGFP2 sensor to track redox changes based on GSH/GSSG
446 allows a fast and selective assessment of redox fluctuations in real time [47], with improved dynamics
447 compared to other redox sensors like roGFP1/roGFP2[71]. Considering that Ca^{2+} mobilization is also a
448 fast event, GRX1-roGFP2 is a suitable tool to investigate the dynamic between ROS and Ca^{2+}.
449 Moreover, the fact that GRX1 does not directly interact with H_2O_2 [48] implies this sensor would not
450 interfere with any eventual interaction between H_2O_2 and its potential targets within the parasite or PV.
451 Nevertheless, in all instances expression GRX1-roGFP2 within *T. gondii* parasites was detrimental to
452 asexual replication. This is surprising as the GRX1-based sensor is generally well tolerated, and
453 presents negligible toxicity in neurons[48, 72]. Inactivation of the catalytic domain of GRX1 only
454 partially recovered parasite growth, suggesting that roGFP2 alone is sufficient to influence parasite
455 replication. Cells contain millimolar concentrations of GSH within their cytoplasm and organelles,
456 and in normal redox conditions the cell maintain the majority of this redox buffer molecule in a
457 reduced form ([GSH]>[GHHS])[73]. Parasites overexpressing GRX1 would be expected to affect the
458 normal GSH/GSSG balance. The addition of NAC, a small molecule that can be used to generate
459 GSH, also slowed parasite growth. This supports the hypothesis that the GSH/GSSG ratio can
460 influence parasite replication. Parasites expressing GRX1ser-roGFP2 are likely have altered redox
461 potential due ability of roGFP not fused with an active GRX1 to interact directly with oxidizing
462 molecules like H_2O_2[74].

463 Targeting of the redox sensor to the PV had a greater effect upon parasite asexual growth
464 compare with expression within the parasite's cytosol. During asexual replication within host cells, *T.*
465 *gondii* resides within the PV. This compartment separates the parasite from the host cytoplasm,
466 providing a niche for parasite survival and replication[75]. All signaling molecules from the host must

467 cross the PV in order to reach the parasite. Should an oxidative signal from the host encounter an
468 unusually reductive environment within the PV due the buffering effect of the redox sensor, the signal
469 could be lost before reaching the parasite. Our work adds valuable information about the complex
470 redox system in *Toxoplasma,* and provides the first evidence that parasite replication is sensitive to
471 redox imbalance. Redox clearly has an important role in *Toxoplasma* pathophysiology and we
472 anticipate that the unveiling of this network will guide future covalent drug discovery targeting redox-
473 sensitive chemically reactive cysteines.
474
475 **Material and Methods**
476 **Parasite and host cell culture:** *T. gondii* tachyzoites from strain RH (Type I) lacking hypoxanthine-
477 guanine phosphoribosyl transferase gene (HXGPRT) were cultivated *in vitro* on monolayers of
478 primary human foreskin fibroblast (HFF, ATTC®) in a humidified incubator at 37°C, 5% CO_2, 3% O_2
479 atmosphere and maintained in Dulbecco's Modified Eagle medium (DMEM) supplemented with 10%
480 of foetal bovine serum (FBS) and 2mM L-glutamine, without antibiotics. All culture were tested
481 against *Mycoplasma* infection on a monthly basis.
482
483 **Generation of plasmids and transgenic parasites:** All primers used in this study are listed in table
484 supplement 2. The GRX1-roGFP2 sensor[47, 76] was amplified from the commercially available vector
485 pEIGW-GRX1-roGFP2 (Addgene plasmid nº64990) using primers 1/2 and insert into digested (HF-
486 EcoRI & PacI) pTUB8 vector containing selectable marker for HXGPRT using Gibson Assembly®
487 Master Mix. The same strategy was used for GRA8-GRX1-roGFP2, using primers 2/3. To generate
488 vectors with the inactivated GRX1 catalytic domain ($GRX1_{cys23-26}$)[77, 78], primers 4/5 were used to
489 replace cysteine with a serine on pTUB8::GRX1-roGFP2 and primers 4/6 on pTUB8::GRA8-GRX1-
490 roGFP2, followed circularization with KLD reaction mix (NEB), resulting the vectors
491 pTUB8::$GRX1_{(ser23-26)}$-roGFP2 and pTUB8::GRA8-$GRX1_{(ser23-26)}$-roGFP2. All vectors were linearized
492 and transfected into RHΔ*ku80*Δ*HXGPRT* parasites as previously described[79]. Transfected parasites
493 were selected 24 hrs post-transfection by addition of mycophenolic acid (MPA; 25µg/mL) and
494 xanthine (XAN; 50 µg/mL) to culture medium. Strains were cloned by limiting dilution into 96 well

495 plates, and five clones selected. Genomic DNA was extracted from extracellular tachyzoites using
496 Monarch® Genomic DNA Purification Kit (New England BioLabs). Presence of GRX1-based sensors
497 was confirmed using primer pair 7/8.

498 To generate the calcium sensor construct pUPRT::GFP-T2A-jRCaMP1b, sequence encoding
499 the red fluorescent calcium sensor protein jRCaMP1b[40] was ordered from IDT as a custom synthetic
500 gene, and PCR amplified with appropriate Gibson overhangs using primers 9/10. The 5'UTR of
501 *GRA1* was PCR amplified from pTKO2c[80] using primers 11/12, and the GFP-T2A fusion sequence
502 was amplified from an unpublished in-house plasmid using primers 13/14. All three fragments were
503 subsequently cloned by Gibson assembly into PacI-digested UPRT targeting vector pUPRT-HA[81].
504 The resulting construct was linearised using NaeI and transfected into RH Δ*ku80*Δ*hxgprt* parasites to
505 generate the GFP-T2A-jRCaMP1b calcium sensor line. Transgenic parasites were subjected to 5'-
506 fluo-2'-deoxyuridine (FUDR) selection (5 μM) 24 hrs after transfection. To generate the GFP-T2A-
507 jRCaMP1b Δ*CDPK3* line, the *HXGPRT* casette (flanked by 5' and 3' DHFR UTR sequences) was
508 PCR amplified from *pGRA*-HA_HXGPRT[82] using primers 15/16 (introducing 40bp CDPK3
509 homology regions to the amplified fragment) and co-transfected into RH Δ*ku80*Δ*HXGPRT* with
510 pSag1::Cas9-U6::dbl-sgCDPK3. The pSag1::Cas9-U6::dbl-sgCDPK3 vector was generated by
511 inverse PCR amplification of the pSag1::Cas9-U6[83] vector using primer pairs 17/18 and 17/19 to
512 generate intermediate constructs pSag1::Cas9-U6::sg1CDPK3 (comprising sgRNA1) and
513 pSag1::Cas9-U6::sg2CDPK3 (comprising sgRNA2) respectively. Following circularization of both
514 intermediate constructs using KLD reaction mix, a region comprising sgRNA1 was PCR amplified
515 with primers 20/21 from pSag1::Cas9-U6::sg1CDPK3 and Gibson assembled into Kpn1/XhoI
516 linearised pSag1::Cas9-U6:: sg2CDPK3 to generate the double sgRNA plasmid pSag1::Cas9-U6::dbl-
517 sgCDPK3. Recombinant parasites were selected 24 hrs post transfection as previously described for
518 GRX1-roGFP2. Integration of the HXGPRT cassette at the CDPK3 locus was confirmed using primer
519 pairs 22/23 and 24/25 to confirm 5' and 3' integration respectively. Absence of the endogenous
520 CDPK3 locus was confirmed using primers 26/27. RH-GFP-Luc parasites (expressing GFP mutant 3
521 and firefly luciferase IAV[84]) were a gift from Dr Moritz Treeck.
522

523 **Identification of *T. gondii* genes related to redox:** Within the *Toxoplasma* database (ToxoDB[85]), a
524 list of genes related to redox signaling in *T. gondii* were obtained using the keywords "thioredoxin",
525 "glutathione", "glutaredoxin", "peroxiredoxin" and "protein disulfide" on gene text search option.
526 The function domains of the canonical antioxidant groups Trxs, Grx-GSH, Prxs and PDIs were
527 confirmed for each gene using Basic Local Alignment Search Tool (BLAST) at National Center for
528 Biotechnology information (NCBI) database (www.ncbi.nlm.nih.gov/). The spatial protein
529 localization related to each redox gene were extracted from the localisation of organelle proteins by
530 isotope tagging (hyperLOPIT)[37, 86] dataset available through ToxoDB.
531
532 **Plaque and replication assays:** For plaque assays, tachyzoites were harvested from infected HFF by
533 syringe passage followed by filtration (5µm). ~100 tachyzoites were added per well of a 6-well plate
534 prepared with confluent HFF monolayers, and allowed to grow undisturbed for 6 days. Plates were
535 washed with phosphate-buffer saline (PBS) and fixed with cold methanol, stained with crystal violet
536 and scanned. Plaque counts and area measurements were performed using FIJI software by drawing
537 region of interesting (ROI). For replication assays, the freshly lysed tachyzoites were added to HFF
538 monolayers grown on a µ-slide 8 well glass bottom chamber (Ibidi®) with multiplicity of infection
539 (MOI) 1. To synchronize in the infection, parasites were allowed to settle onto chilled host cells for
540 20 minutes, and then allowed to invade for 2 hours at 37˚C. Cells were washed with PBS to remove
541 extracellular tachyzoites. Cells were incubated for a further 18 hours, and subsequently fixed with 3%
542 paraformaldehyde at room temperature (RT) for 20 min, and blocked with PBS supplemented with 2%
543 FBS. Parasites per vacuole were counted by excitation with 470nm laser (4% intensity) widefield
544 Nikon Eclipse Ti-E inverted microscope equipped with an ORCA- Flash4.0 camera (Hamamatsu,
545 Japan) and NIS-Elements Viewer software (Nikon), 60x-oil objective. All parasite strains were
546 genetically encoding for GFP or roGFP2. All strains were tested tree independent times, each with
547 three technical replicates.
548
549 **Egress assay:** Freshly lysed tachyzoites from RH-GFP-t2a-jRCaMP1b parasites were harvested and
550 inoculated (MOI:1) onto confluent HFF cells grown on 24 well plates, and grown for 18 hours. Cells

551 were washed with PBS and the growth medium replaced with phenol red free DMEM without FBS
552 and incubate for a further three hours. Medium was removed and cells were incubated for 30 minutes
553 with PBS plus drugs (A23187, R59022, H_2O_2) or vehicle controls (water, DMSO). At the end of
554 incubation, the supernatant of the wells was carefully aspirated and cells were detached by 10 min
555 incubation with 200 µL of RT Accutase™. Accutase-release cell suspensions were fixed with 200 µL
556 of 8% paraformaldehyde (20 minutes, RT). Fixed cells were transferred into falcon 5 mL tube with 35
557 µm nylon mesh cap. Free fluorescent parasite and infected HFF population were analysed and
558 quantified in a BD LRSFortessa™. A total of 5000 events were collected for each tube. Blue laser
559 (488nm) with 530/30 nm filter was used to detect the GFP signal. An uninfected HFF control was
560 used to assess the effect of each drug treatment on host cell gating. Each drug condition was tested
561 two independent times, each with six technical replicates.
562
563 **Fluorescence microscopy:** For cytosolic Ca^{2+} fluorometric measurements, RH-GFP-t2a-jRCaMP1b
564 or RH-GFP-t2a-jRCaMP1bΔCDPK3 parasites were added (MOI:1) to confluent HFF grown on 8 well
565 glass bottom chamber, and allowed to grow for 18 hours. Wells were washed with PBS and media
566 replaced by phenol red DMEM medium without FBS, and incubate for a further two hours. Images of
567 live infected HFFs were captured at 37°C, using a 60x-oil objective in the same widefield microscope
568 previously describe on replication assay. GFP (470 nm excitation/ 520 nm emission) and jRCaMP1b
569 (555 nm excitation/ 605 nm emission) with 100 milliseconds acquisition rate signal were collected
570 every second for up to a maximum 10 minutes. Drugs were applied on the wells after one minute of
571 acquisition by pipetting. Image analyses were performed using FIJI software. Raw fluorescence
572 readout (F) for each vacuole on each channel was normalised against the average of the baseline
573 signal before adding the drug (F_0) using the ratio F/F_0 bringing the resting baseline value to one. To
574 distinguish intracellular Ca^{2+} oscillation signal from vacuole movement, the $F_{(jRCaMP1b)}/F_{0(jRCaMP1b)}$
575 values were normalised against the GFP signal $F_{(GFP)}/F_{0(GFP)}$. Ca^{2+} response during a specific time is
576 given by the formula: $(F_{(jRCaMP1b)}/F_{0(jRCaMP1b)}) / (F_{(GFP)}/F_{0(GFP)})$.
577 For redox measurements, parasites expressing ratiometric GRX1 based sensors were treated as
578 described for RH-GFP-t2a-jRCaMP1b parasites. Oxidized GRX1-roGFP2 (395 nm excitation/ 520

579 nm emission) and reduced GRX1-roGFP2 (470 nm excitation/ 520 nm emission) with 200
580 milliseconds acquisition rate signal were collected every second for up to a maximum 10 minutes.
581 Data analyses is similar to Ca^{2+}, the redox reading was obtained by formula: $(F_{(oxidised)}/F_{0(oxidised)})$ /
582 $(F_{(reduced)}/F_{0(reduced)})$.
583
584 **Chemical and Reagents:** Hydrogen peroxide 30% (w/w) solution with stabilizer; diacylglycerol
585 kinase inhibitor (R59022); A23187, Ionomycin, anhydrous methanol, and crystal violet solution were
586 obtained from Sigma-Aldrich Company Ltd. α-tocopherol phosphate disodium salt from Merk.
587 Dimethylsulfoxide (DMSO) anhydrous and paraformaldehyde 16% solution from Life Technologies.
588 Accutase cell detachment solution from Fisher Scientific Ltd.

589 **Statistical Analysis:** The data are represented as the mean ± SEM and analysed using two-tailed
590 pared Student *t* test between two groups and one-way or 2way analyses of variance (ANOVA) with
591 Bonferroni's multiple comparisons test for comparing means between ≥3. All data were analysed
592 using GraphPad Prism 9 software (California, USA). The data were considered statistically significant
593 when P values <0.05.
594
595 **Funding**
596 This work was supported by grant 202553/Z/16/Z from the Wellcome Trust & Royal Society (to
597 MAC), and BB/M011178/1 from the BBSRC (to HJB and MAC).
598
599 **Acknowledgements**
600 We sincerely thank Prof Jake Baum and Dr George Ashdown for the access and assistance to
601 widefield microscopy, Dr Moritz Treeck for the RH-GFP-Luc line, Dr Lilach Sheiner for the roGFP
602 construct, and Dr Gautam Dey for useful discussions. We would also like to thank the Imperial
603 College Flow Cytometry Facility team in South Kensington for technical support.
604
605

606 **Competing interests**

607 The authors have declared there are no conflict or competing interest.

608

609 **References**

610 1. Halonen SK, Weiss LM. Toxoplasmosis. Handb Clin Neurol. 2013;114:125-45.

611 2. Flegr J, Prandota J, Sovickova M, Israili ZH. Toxoplasmosis--a global threat. Correlation of
612 latent toxoplasmosis with specific disease burden in a set of 88 countries. PLoS One.
613 2014;9(3):e90203.

614 3. Sheffield HG, Melton ML. The fine structure and reproduction of Toxoplasma gondii. J
615 Parasitol. 1968;54(2):209-26.

616 4. Dubey JP. WAAP and Pfizer Award for excellence in veterinary parasitology research.
617 Pursuing life cycles and transmission of cyst-forming coccidia of animals and humans. Vet Parasitol.
618 1996;64(1-2):13-20.

619 5. Weiss LM, Dubey JP. Toxoplasmosis: A history of clinical observations. Int J Parasitol.
620 2009;39(8):895-901.

621 6. Luft BJ, Remington JS. Toxoplasmic encephalitis in AIDS. Clin Infect Dis. 1992;15(2):211-
622 22.

623 7. Goldman M, Carver RK, Sulzer AJ. Reproduction of Toxoplasma gondii by internal budding.
624 J Parasitol. 1958;44(2):161-71.

625 8. Montoya JG, Liesenfeld O. Toxoplasmosis. Lancet. 2004;363(9425):1965-76.

626 9. Lourido S, Moreno SN. The calcium signaling toolkit of the Apicomplexan parasites
627 Toxoplasma gondii and Plasmodium spp. Cell calcium. 2015;57(3):186-93.

628 10. Vieira MC, Moreno SN. Mobilization of intracellular calcium upon attachment of
629 Toxoplasma gondii tachyzoites to human fibroblasts is required for invasion. Mol Biochem Parasitol.
630 2000;106(1):157-62.

631 11. Pace DA, McKnight CA, Liu J, Jimenez V, Moreno SN. Calcium entry in Toxoplasma gondii
632 and its enhancing effect of invasion-linked traits. J Biol Chem. 2014;289(28):19637-47.

633 12. Wetzel DM, Chen LA, Ruiz FA, Moreno SN, Sibley LD. Calcium-mediated protein secretion
634 potentiates motility in Toxoplasma gondii. J Cell Sci. 2004;117(Pt 24):5739-48.
635 13. Endo T, Sethi KK, Piekarski G. Toxoplasma gondii: calcium ionophore A23187-mediated
636 exit of trophozoites from infected murine macrophages. Exp Parasitol. 1982;53(2):179-88.
637 14. Murphy RC, Ojo KK, Larson ET, Castellanos-Gonzalez A, Perera BG, Keyloun KR, et al.
638 Discovery of Potent and Selective Inhibitors of Calcium-Dependent Protein Kinase 1 (CDPK1) from
639 C. parvum and T. gondii. ACS Med Chem Lett. 2010;1(7):331-5.
640 15. Ojo KK, Larson ET, Keyloun KR, Castaneda LJ, Derocher AE, Inampudi KK, et al.
641 Toxoplasma gondii calcium-dependent protein kinase 1 is a target for selective kinase inhibitors.
642 Nature structural & molecular biology. 2010;17(5):602-7.
643 16. Garrison E, Treeck M, Ehret E, Butz H, Garbuz T, Oswald BP, et al. A forward genetic
644 screen reveals that calcium-dependent protein kinase 3 regulates egress in Toxoplasma. PLoS Pathog.
645 2012;8(11):e1003049.
646 17. Bullen HE, Jia Y, Yamaryo-Botte Y, Bisio H, Zhang O, Jemelin NK, et al. Phosphatidic
647 Acid-Mediated Signaling Regulates Microneme Secretion in Toxoplasma. Cell Host Microbe.
648 2016;19(3):349-60.
649 18. Brown KM, Lourido S, Sibley LD. Serum Albumin Stimulates Protein Kinase G-dependent
650 Microneme Secretion in Toxoplasma gondii. J Biol Chem. 2016;291(18):9554-65.
651 19. Guzik TJ, West NE, Black E, McDonald D, Ratnatunga C, Pillai R, et al. Vascular superoxide
652 production by NAD(P)H oxidase: association with endothelial dysfunction and clinical risk factors.
653 Circ Res. 2000;86(9):E85-90.
654 20. Winterbourn CC, Hampton MB. Thiol chemistry and specificity in redox signaling. Free
655 Radic Biol Med. 2008;45(5):549-61.
656 21. Pastore A, Piemonte F. S-Glutathionylation signaling in cell biology: progress and prospects.
657 Eur J Pharm Sci. 2012;46(5):279-92.
658 22. Popov D. Protein S-glutathionylation: from current basics to targeted modifications. Arch
659 Physiol Biochem. 2014;120(4):123-30.

660 23. Sabens Liedhegner EA, Gao XH, Mieyal JJ. Mechanisms of altered redox regulation in
661 neurodegenerative diseases--focus on S--glutathionylation. Antioxid Redox Signal. 2012;16(6):543-
662 66.
663 24. Xiong Y, Uys JD, Tew KD, Townsend DM. S-glutathionylation: from molecular mechanisms
664 to health outcomes. Antioxid Redox Signal. 2011;15(1):233-70.
665 25. Murray HW, Cohn ZA. Macrophage oxygen-dependent antimicrobial activity. I.
666 Susceptibility of Toxoplasma gondii to oxygen intermediates. J Exp Med. 1979;150(4):938-49.
667 26. Ding M, Kwok LY, Schluter D, Clayton C, Soldati D. The antioxidant systems in
668 Toxoplasma gondii and the role of cytosolic catalase in defence against oxidative injury. Mol
669 Microbiol. 2004;51(1):47-61.
670 27. Luder CG, Gross U. Apoptosis and its modulation during infection with Toxoplasma gondii:
671 molecular mechanisms and role in pathogenesis. Curr Top Microbiol Immunol. 2005;289:219-37.
672 28. Luder CG, Stanway RR, Chaussepied M, Langsley G, Heussler VT. Intracellular survival of
673 apicomplexan parasites and host cell modification. Int J Parasitol. 2009;39(2):163-73.
674 29. Akerman SE, Muller S. Peroxiredoxin-linked detoxification of hydroperoxides in
675 Toxoplasma gondii. J Biol Chem. 2005;280(1):564-70.
676 30. Kaasch AJ, Joiner KA. Targeting and subcellular localization of Toxoplasma gondii catalase.
677 Identification of peroxisomes in an apicomplexan parasite. J Biol Chem. 2000;275(2):1112-8.
678 31. Stommel EW, Ely KH, Schwartzman JD, Kasper LH. Toxoplasma gondii: dithiol-induced
679 Ca2+ flux causes egress of parasites from the parasitophorous vacuole. Exp Parasitol. 1997;87(2):88-
680 97.
681 32. Silverman JA, Qi H, Riehl A, Beckers C, Nakaar V, Joiner KA. Induced activation of the
682 Toxoplasma gondii nucleoside triphosphate hydrolase leads to depletion of host cell ATP levels and
683 rapid exit of intracellular parasites from infected cells. J Biol Chem. 1998;273(20):12352-9.
684 33. Child MA, Garland M, Foe I, Madzelan P, Treeck M, van der Linden WA, et al. Toxoplasma
685 DJ-1 Regulates Organelle Secretion by a Direct Interaction with Calcium-Dependent Protein Kinase 1.
686 mBio. 2017;8(1).

687 34. Augusto L, Martynowicz J, Amin PH, Carlson KR, Wek RC, Sullivan WJ. TgIF2K-B is an
688 eIF2α kinase in Toxoplasma gondii that responds to oxidative stress and optimizes
689 pathogenicity. bioRxiv. 2020:2020.09.24.312744.
690 35. Odberg-Ferragut C, Renault JP, Viscogliosi E, Toursel C, Briche I, Engels A, et al. Molecular
691 cloning, expression analysis and iron metal cofactor characterisation of a superoxide dismutase from
692 Toxoplasma gondii. Mol Biochem Parasitol. 2000;106(1):121-9.
693 36. Sibley LD, Lawson R, Weidner E. Superoxide dismutase and catalase in Toxoplasma gondii.
694 Mol Biochem Parasitol. 1986;19(1):83-7.
695 37. Barylyuk K, Koreny L, Ke H, Butterworth S, Crook OM, Lassadi I, et al. A Comprehensive
696 Subcellular Atlas of the Toxoplasma Proteome via hyperLOPIT Provides Spatial Context for Protein
697 Functions. Cell Host Microbe. 2020;28(5):752-66 e9.
698 38. Meissner G. Regulation of mammalian ryanodine receptors. Front Biosci. 2002;7:d2072-80.
699 39. Oda T, Yang Y, Uchinoumi H, Thomas DD, Chen-Izu Y, Kato T, et al. Oxidation of
700 ryanodine receptor (RyR) and calmodulin enhance Ca release and pathologically alter, RyR structure
701 and calmodulin affinity. J Mol Cell Cardiol. 2015;85:240-8.
702 40. Dana H, Mohar B, Sun Y, Narayan S, Gordus A, Hasseman JP, et al. Sensitive red protein
703 calcium indicators for imaging neural activity. Elife. 2016;5.
704 41. Black MW, Arrizabalaga G, Boothroyd JC. Ionophore-resistant mutants of Toxoplasma
705 gondii reveal host cell permeabilization as an early event in egress. Mol Cell Biol. 2000;20(24):9399-
706 408.
707 42. Treeck M, Sanders JL, Gaji RY, LaFavers KA, Child MA, Arrizabalaga G, et al. The
708 calcium-dependent protein kinase 3 of toxoplasma influences basal calcium levels and functions
709 beyond egress as revealed by quantitative phosphoproteome analysis. PLoS Pathog.
710 2014;10(6):e1004197.
711 43. Stewart RJ, Whitehead L, Nijagal B, Sleebs BE, Lessene G, McConville MJ, et al. Analysis
712 of Ca(2)(+) mediated signaling regulating Toxoplasma infectivity reveals complex relationships
713 between key molecules. Cell Microbiol. 2017;19(4).

714 44. Cooke E, Al-Mohanna FA, Hallett MB. Diacylglycerol kinase inhibitor, R59022, potentiates
715 neutrophil oxidase activation by Ca2+-dependent stimuli. Evidence for two separate but convergent
716 pathways. Biochem Pharmacol. 1987;36(20):3459-62.
717 45. Bullen HE, Bisio H, Soldati-Favre D. The triumvirate of signaling molecules controlling
718 Toxoplasma microneme exocytosis: Cyclic GMP, calcium, and phosphatidic acid. PLoS Pathog.
719 2019;15(5):e1007670.
720 46. Carey KL, Donahue CG, Ward GE. Identification and molecular characterization of GRA8, a
721 novel, proline-rich, dense granule protein of Toxoplasma gondii. Mol Biochem Parasitol.
722 2000;105(1):25-37.
723 47. Aller I, Rouhier N, Meyer AJ. Development of roGFP2-derived redox probes for
724 measurement of the glutathione redox potential in the cytosol of severely glutathione-deficient rml1
725 seedlings. Front Plant Sci. 2013;4:506.
726 48. Gutscher M, Pauleau AL, Marty L, Brach T, Wabnitz GH, Samstag Y, et al. Real-time
727 imaging of the intracellular glutathione redox potential. Nat Methods. 2008;5(6):553-9.
728 49. Laporte D, Olate E, Salinas P, Salazar M, Jordana X, Holuigue L. Glutaredoxin GRXS13
729 plays a key role in protection against photooxidative stress in Arabidopsis. J Exp Bot.
730 2012;63(1):503-15.
731 50. Ezerina D, Takano Y, Hanaoka K, Urano Y, Dick TP. N-Acetyl Cysteine Functions as a Fast-
732 Acting Antioxidant by Triggering Intracellular H2S and Sulfane Sulfur Production. Cell Chem Biol.
733 2018;25(4):447-59 e4.
734 51. Dupre-Crochet S, Erard M, Nubetae O. ROS production in phagocytes: why, when, and
735 where? J Leukoc Biol. 2013;94(4):657-70.
736 52. McLeod R, Estes R, Mack DG, McLeod EG. Effects of human alveolar macrophages and
737 peripheral blood monocytes on Toxoplasma gondii. J Infect Dis. 1983;147(5):957.
738 53. Sibley LD, Krahenbuhl JL, Weidner E. Lymphokine activation of J774G8 cells and mouse
739 peritoneal macrophages challenged with Toxoplasma gondii. Infect Immun. 1985;49(3):760-4.

740 54. Wilson CB, Tsai V, Remington JS. Failure to trigger the oxidative metabolic burst by normal
741 macrophages: possible mechanism for survival of intracellular pathogens. J Exp Med.
742 1980;151(2):328-46.
743 55. Shrestha SP, Tomita T, Weiss LM, Orlofsky A. Proliferation of Toxoplasma gondii in
744 inflammatory macrophages in vivo is associated with diminished oxygen radical production in the
745 host cell. Int J Parasitol. 2006;36(4):433-41.
746 56. Lima TS, Lodoen MB. Mechanisms of Human Innate Immune Evasion by Toxoplasma
747 gondii. Front Cell Infect Microbiol. 2019;9:103.
748 57. Veal E, Day A. Hydrogen peroxide as a signaling molecule. Antioxid Redox Signal.
749 2011;15(1):147-51.
750 58. Sautel CF, Ortet P, Saksouk N, Kieffer S, Garin J, Bastien O, et al. The histone methylase
751 KMTox interacts with the redox-sensor peroxiredoxin-1 and targets genes involved in Toxoplasma
752 gondii antioxidant defences. Mol Microbiol. 2009;71(1):212-26.
753 59. Biddau M, Bouchut A, Major J, Saveria T, Tottey J, Oka O, et al. Two essential Thioredoxins
754 mediate apicoplast biogenesis, protein import, and gene expression in Toxoplasma gondii. PLoS
755 Pathog. 2018;14(2):e1006836.
756 60. Xue J, Jiang W, Chen Y, Gong F, Wang M, Zeng P, et al. Thioredoxin reductase from
757 Toxoplasma gondii: an essential virulence effector with antioxidant function. FASEB J.
758 2017;31(10):4447-57.
759 61. Volk T, Hensel M, Kox WJ. Transient Ca2+ changes in endothelial cells induced by low
760 doses of reactive oxygen species: role of hydrogen peroxide. Mol Cell Biochem. 1997;171(1-2):11-21.
761 62. Avdonin PV, Nadeev AD, Tsitrin EB, Tsitrina AA, Avdonin PP, Mironova GY, et al.
762 Involvement of two-pore channels in hydrogen peroxide-induced increase in the level of calcium ions
763 in the cytoplasm of human umbilical vein endothelial cells. Dokl Biochem Biophys. 2017;474(1):209-
764 12.
765 63. Roveri A, Coassin M, Maiorino M, Zamburlini A, van Amsterdam FT, Ratti E, et al. Effect of
766 hydrogen peroxide on calcium homeostasis in smooth muscle cells. Arch Biochem Biophys.
767 1992;297(2):265-70.

768 64. Di Virgilio F, Steinberg TH, Silverstein SC. Inhibition of Fura-2 sequestration and secretion
769 with organic anion transport blockers. Cell Calcium. 1990;11(2-3):57-62.
770 65. Carter SB. Effects of cytochalasins on mammalian cells. Nature. 1967;213(5073):261-4.
771 66. Hyslop PA, Hinshaw DB, Scraufstatter IU, Cochrane CG, Kunz S, Vosbeck K. Hydrogen
772 peroxide as a potent bacteriostatic antibiotic: implications for host defense. Free Radic Biol Med.
773 1995;19(1):31-7.
774 67. Gutscher M, Sobotta MC, Wabnitz GH, Ballikaya S, Meyer AJ, Samstag Y, et al. Proximity-
775 based protein thiol oxidation by H2O2-scavenging peroxidases. J Biol Chem. 2009;284(46):31532-40.
776 68. Nagamune K, Sibley LD. Comparative genomic and phylogenetic analyses of calcium
777 ATPases and calcium-regulated proteins in the apicomplexa. Mol Biol Evol. 2006;23(8):1613-27.
778 69. Wu F, Chi Y, Jiang Z, Xu Y, Xie L, Huang F, et al. Hydrogen peroxide sensor HPCA1 is an
779 LRR receptor kinase in Arabidopsis. Nature. 2020;578(7796):577-81.
780 70. Lovett JL, Marchesini N, Moreno SN, Sibley LD. Toxoplasma gondii microneme secretion
781 involves intracellular Ca(2+) release from inositol 1,4,5-triphosphate (IP(3))/ryanodine-sensitive
782 stores. J Biol Chem. 2002;277(29):25870-6.
783 71. Hanson GT, Aggeler R, Oglesbee D, Cannon M, Capaldi RA, Tsien RY, et al. Investigating
784 mitochondrial redox potential with redox-sensitive green fluorescent protein indicators. J Biol Chem.
785 2004;279(13):13044-53.
786 72. Hasel P, McKay S, Qiu J, Hardingham GE. Selective dendritic susceptibility to bioenergetic,
787 excitotoxic and redox perturbations in cortical neurons. Biochim Biophys Acta. 2015;1853(9):2066-
788 76.
789 73. Brieger K, Schiavone S, Miller FJ, Jr., Krause KH. Reactive oxygen species: from health to
790 disease. Swiss Med Wkly. 2012;142:w13659.
791 74. Liu X, Wu J, Liu H, Zong N, Zhao J. RoGFP1 is a quantitative biosensor in maize cells for
792 cellular redox changes caused by environmental and endogenous stimuli. Biochem Biophys Res
793 Commun. 2014;452(3):503-8.
794 75. Clough B, Frickel EM. The Toxoplasma Parasitophorous Vacuole: An Evolving Host-
795 Parasite Frontier. Trends Parasitol. 2017;33(6):473-88.

796 76. Meyer AJ, Brach T, Marty L, Kreye S, Rouhier N, Jacquot JP, et al. Redox-sensitive GFP in
797 Arabidopsis thaliana is a quantitative biosensor for the redox potential of the cellular glutathione
798 redox buffer. Plant J. 2007;52(5):973-86.
799 77. Sun C, Berardi MJ, Bushweller JH. The NMR solution structure of human glutaredoxin in the
800 fully reduced form. J Mol Biol. 1998;280(4):687-701.
801 78. Yang Y, Jao S, Nanduri S, Starke DW, Mieyal JJ, Qin J. Reactivity of the human
802 thioltransferase (glutaredoxin) C7S, C25S, C78S, C82S mutant and NMR solution structure of its
803 glutathionyl mixed disulfide intermediate reflect catalytic specificity. Biochemistry.
804 1998;37(49):17145-56.
805 79. Soldati D, Boothroyd JC. Transient transfection and expression in the obligate intracellular
806 parasite Toxoplasma gondii. Science. 1993;260(5106):349-52.
807 80. Caffaro CE, Koshy AA, Liu L, Zeiner GM, Hirschberg CB, Boothroyd JC. A nucleotide
808 sugar transporter involved in glycosylation of the Toxoplasma tissue cyst wall is required for efficient
809 persistence of bradyzoites. PLoS Pathog. 2013;9(5):e1003331.
810 81. Reese ML, Zeiner GM, Saeij JP, Boothroyd JC, Boyle JP. Polymorphic family of injected
811 pseudokinases is paramount in Toxoplasma virulence. Proc Natl Acad Sci U S A. 2011;108(23):9625-
812 30.
813 82. Coppens I, Dunn JD, Romano JD, Pypaert M, Zhang H, Boothroyd JC, et al. Toxoplasma
814 gondii sequesters lysosomes from mammalian hosts in the vacuolar space. Cell. 2006;125(2):261-74.
815 83. Behnke MS, Zhang TP, Dubey JP, Sibley LD. Toxoplasma gondii merozoite gene expression
816 analysis with comparison to the life cycle discloses a unique expression state during enteric
817 development. BMC Genomics. 2014;15:350.
818 84. Ploemen IH, Prudencio M, Douradinha BG, Ramesar J, Fonager J, van Gemert GJ, et al.
819 Visualisation and quantitative analysis of the rodent malaria liver stage by real time imaging. PLoS
820 One. 2009;4(11):e7881.
821 85. Gajria B, Bahl A, Brestelli J, Dommer J, Fischer S, Gao X, et al. ToxoDB: an integrated
822 Toxoplasma gondii database resource. Nucleic Acids Res. 2008;36(Database issue):D553-6.

86. Crook OM, Mulvey CM, Kirk PDW, Lilley KS, Gatto L. A Bayesian mixture modelling approach for spatial proteomics. PLoS Comput Biol. 2018;14(11):e1006516.

851 **Supplement Material**
852

Gene ID (ToxoDB)	Gene annotation	Predicted localisation
TGME49_204480	thioredoxin domain-containing protein	apicoplast
TGME49_209950	thioredoxin domain-containing protein	apicoplast
TGME49_216510	thioredoxin, putative	mitochondria-membrane
TGME49_218530	PITH domain-containing protein	cytosol
TGME49_224060	thioredoxin, putative	golgi
TGME49_247350	thioredoxin domain-containing protein	ER
TGME49_247660	thioredoxin domain-containing protein	NA
TGME49_255480	thioredoxin domain-containing protein	NA
TGME49_266620	thioredoxin domain-containing protein	ER
TGME49_270120	thioredoxin-like protein, TLP1	mitochondria-soluble
TGME49_289180	thioredoxin domain-containing protein	mitochondria-soluble
TGME49_290260	PITH domain-containing protein	cytosol
TGME49_291810	thioredoxin domain-containing protein	NA
TGME49_293870	thioredoxin	cytosol
TGME49_308050	phosducin domain-containing protein	NA
TGME49_309730	thioredoxin reductase	cytosol
TGME49_247025	PITH domain-containing protein	NA
TGME49_258826	thioredoxin domain-containing protein	ER
TGME49_312110	thioredoxin domain-containing protein	apicoplast
TGME49_225060	thioredoxin domain-containing protein	nucleus-chromatin
TGME49_211680	protein disulfide-isomerase	ER
TGME49_218470	protein disulfide-isomerase, putative	NA
TGME49_225790	thioredoxin-like-fold domain-containing protein	cytoskeleton
TGME49_232410	thioredoxin-like-fold domain-containing protein	cytoskeleton
TGME49_238040	protein disulfide-isomerase domain-containing protein	ER
TGME49_249270	protein disulfide isomerase-related protein (provisional), putative	apicoplast
TGME49_226800	GSH-synthase domain-containing protein	nucleolus
TGME49_238070	glutaredoxin domain-containing protein	cytosol
TGME49_247580	glutaredoxin domain-containing protein	rhoptries
TGME49_227150	glutaredoxin domain-containing protein	apicoplast
TGME49_279400	glutaredoxin domain-containing protein	cytosol
TGME49_268730	glutaredoxin domain-containing protein	mitochondria-soluble
TGME49_246920	glutathione reductase	19S proteosome
TGME49_306030	glutathione s-transferase, n-terminal domain containing	ER
TGME49_249630	glutathione s-transferase, N-terminal domain-containing protein	mitochondria-soluble
TGME49_281630	lactamase-b domain-containing protein	nucleolus
TGME49_219130	NADPH-glutathione reductase	apicoplast
TGME49_227100	glutaredoxin domain-containing protein	NA
TGME49_285920	hypothetical protein	NA
TGME49_309210	thioredoxin domain-containing protein / peroxiredoxin 6, putative	cytosol
TGME49_230410	thioredoxin domain-containing protein / peroxiredoxin PRX3	mitochondria-soluble
TGME49_266130	glutathione peroxidase / peroxiredoxin PRX2	NA
TGME49_217890	peroxiredoxin / alkyl hydroperoxide reductase	nucleus
TGME49_286630	peroxiredoxin / redoxin domain-containing protein	apicoplast
TGME49_266120	glutathione peroxidase / thioredoxin-dependent peroxidase TPX1	PM-peripheral
TGME49_316330	superoxide dismutase SOD2	mitochondria-soluble
TGME49_232250	catalase	cytosol
TGME49_316190	superoxide dismutase SOD3	NA
TGME49_316310	superoxide dismutase	cytosol

853 **Table supplement 1:** List of *Toxoplasma gondii* genes related to redox sensing systems and their
854 primary location based on hyperLOPIT datasets. Abbreviations: PITH: proteasome-interacting
855 thioredoxin. ER: endoplasmic reticulum. PM: plasma membrane. GSH: glutathione. NA: not
856 applicable (location not predicted).

857

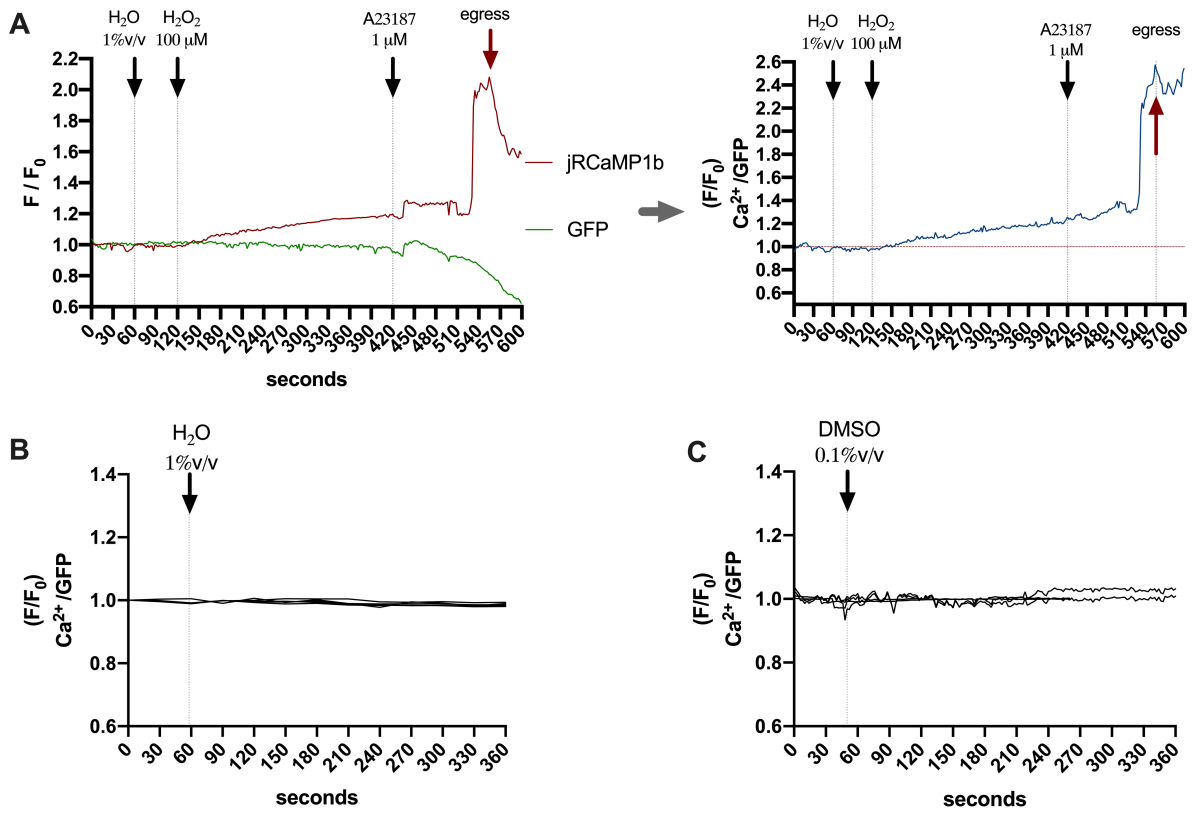

858

859 **Figure supplement 1:** Fluorescence tracking of Ca^{2+} signal and GFP movement on RH-GFP-t2a-
860 jRCaMP1b parasites within host cell. (**A**) Representative trace of parasite vacuoles following
861 treatment with H_2O_2 and ionophore A23187. On left, the graph presents the independent GFP trace
862 (green) and Ca^{2+} signal from jRCaMP1b sensor (red). Note the parasite movement after A23187
863 addition at 420s. On the right graph, the Ca^{2+} signal is normalized to GFP to minimize artefact on the
864 Ca^{2+} measurements due to parasite movement. Red arrow indicates the moment of parasite egress. (**B**)
865 Water, the vehicle solvent for H_2O_2, does not mobilize Ca^{2+}. The graph displays the trace of three
866 independent vacuoles from the same field of view. Data are representative of 15 infected vacuoles
867 from four independent experiments. (**C**) DMSO, the vehicle solvent for ionophore A23187, does not
868 mobilize Ca^{2+}. The graph displays the trace of four independent infected vacuoles from the same field
869 of view. Data are representative of 12 rosettes from three independent experiments. (**A** – **C**): black
870 arrows indicate the time of drug / solvent addition.

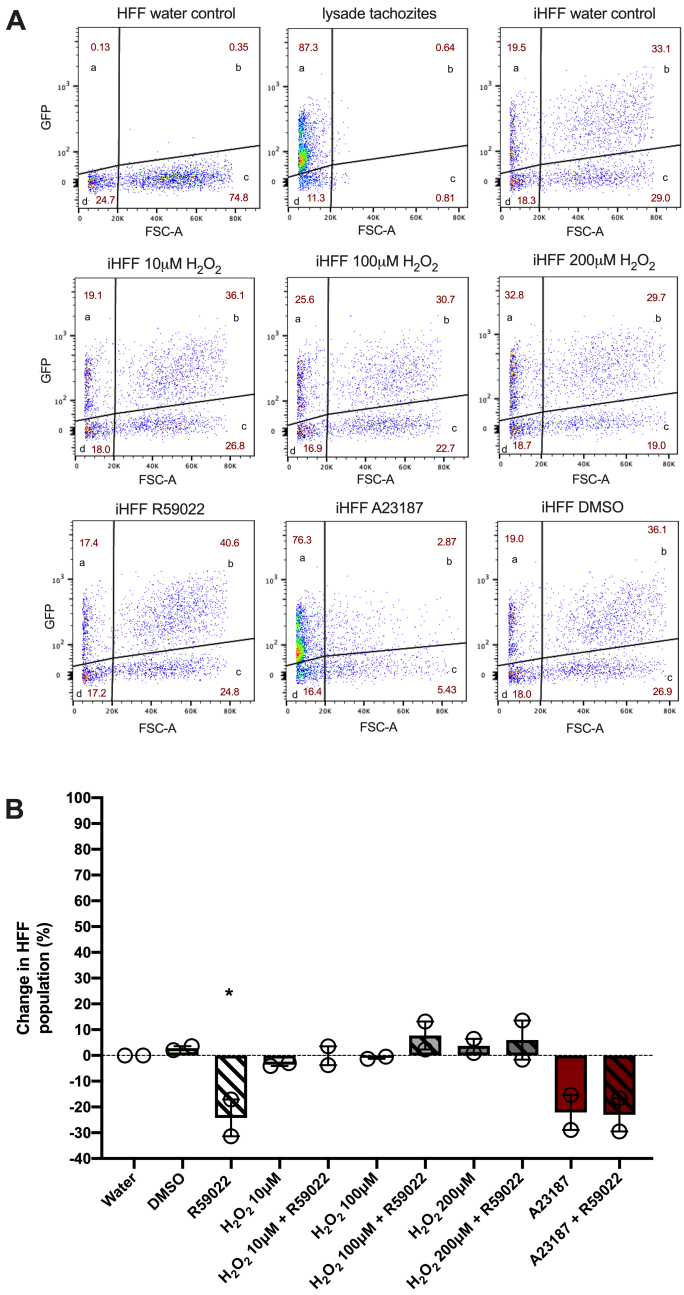

Figure supplement 2: Quantification of RH-GFP-t2a-jCamP1b parasite egress by flow cytometry. (**A**) Representative gating using GFP (Blue laser, 488nm, filter 530/30) against Forward scatter (FSC-A). HFF water control: uninfected human foreskin fibroblast (HFF) are mainly localised in quadrant c. Lysed tachyzoites: free RH-GFP-t2a-jCamP1b parasites are mainly localised in quadrant a. iHFF water control: infected host cells are detected in quadrant b. By using the GFP it is possible to distinguish free fluorescent parasite from iHFF in a population and assess the egress rates throughout different treatments. (**B**) Effect of drug incubation on non-infected HFF. The graph presents a change on event number within the non-fluorescent HFF gate. Data represent the mean ±SEM of two independent experiments, six technical replicates on each. Significance was calculated using one-way Anova, Bonferroni's multiple comparisons P value *< 0.05.

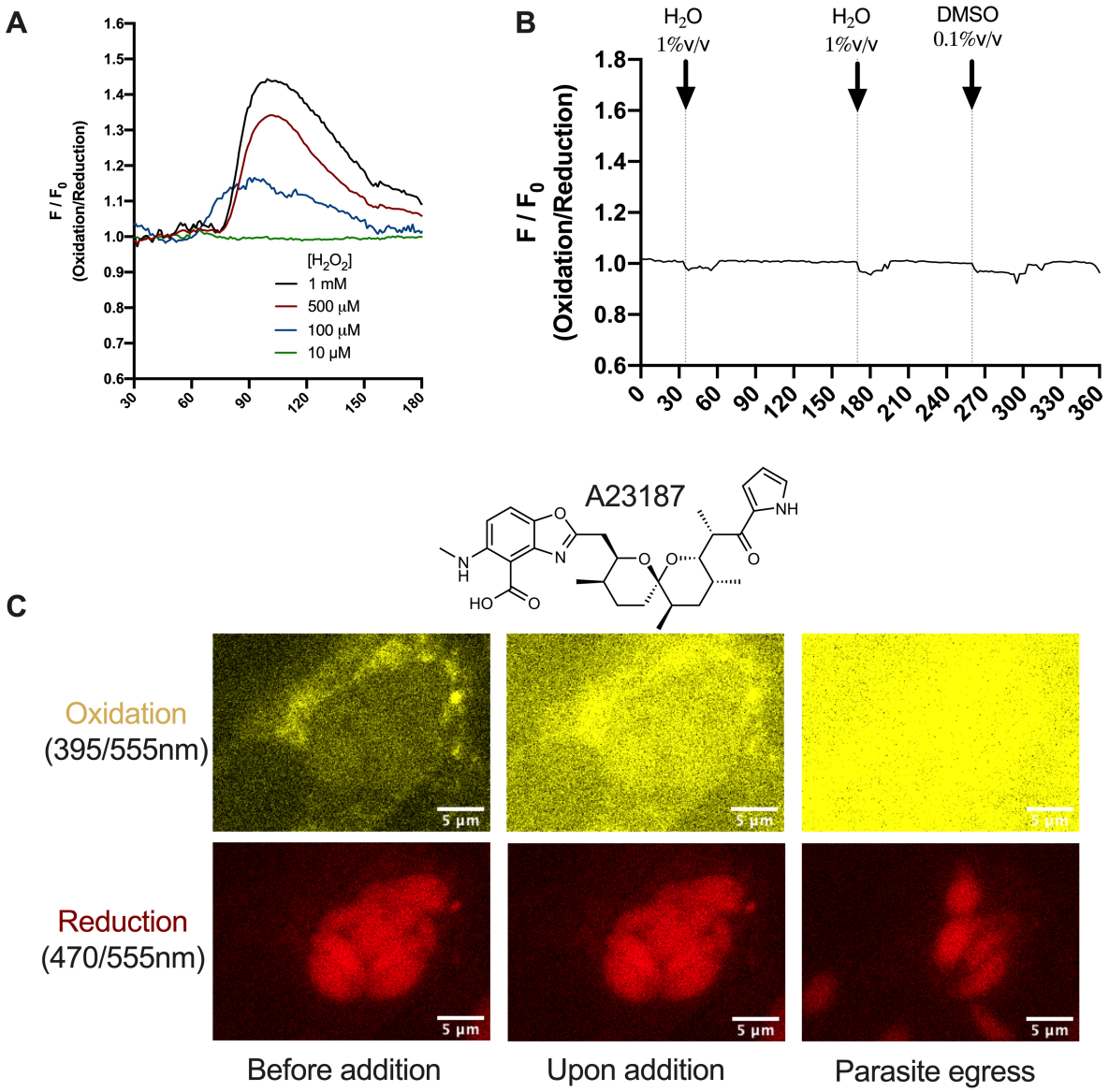

Figure supplement 3: Exploring the redox sensitivity of RH-GRX1-roGFP2 parasites to H_2O_2. (**A**) Tracking the GSH/GSSG change upon different concentration of H_2O_2. Among the concentration tested, 10 µM was the only one that did not induce a change in redox within the parasite cytosol. Data are representative of five infected vacuoles from each concentration, one independent experiment. (**B**) Water (vehicle control for H_2O_2) and DMSO (vehicle control for A23187) do not trigger change in GSH/GSSG. Data are representative of 12 vacuoles from three independent experiments. (**C**) Autofluorescence effect of A23187 drug on oxidation channel makes this ionophore unsuitable for ratiometric analyses of GRX1-roGFP2 sensor. Widefield microscope imaging depicting an egress induce by A23187. The structure of A23187 is shown above microscopy images.

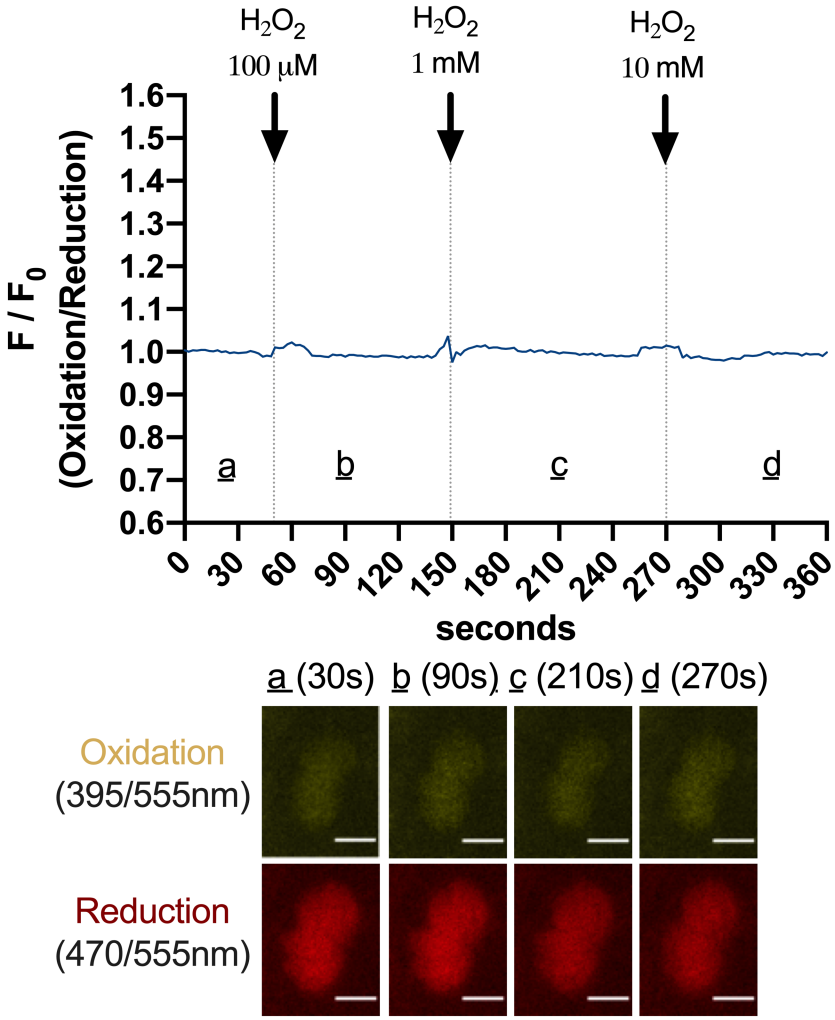

Supplemental Figure 4: Inactivation of the catalytic domain of glutaredoxin 1 makes the GRX1-roGFP2 redox sensor insensitive to changes in GSH/GSSH. Parasite expressing GRX1ser-roGFP2 do not display fluorescent changes in either channel (reduction or oxidation) upon addition of H_2O_2. Data are representative of 12 infected vacuole, three independent experiments. Black arrows indicate the time of H_2O_2 addition.

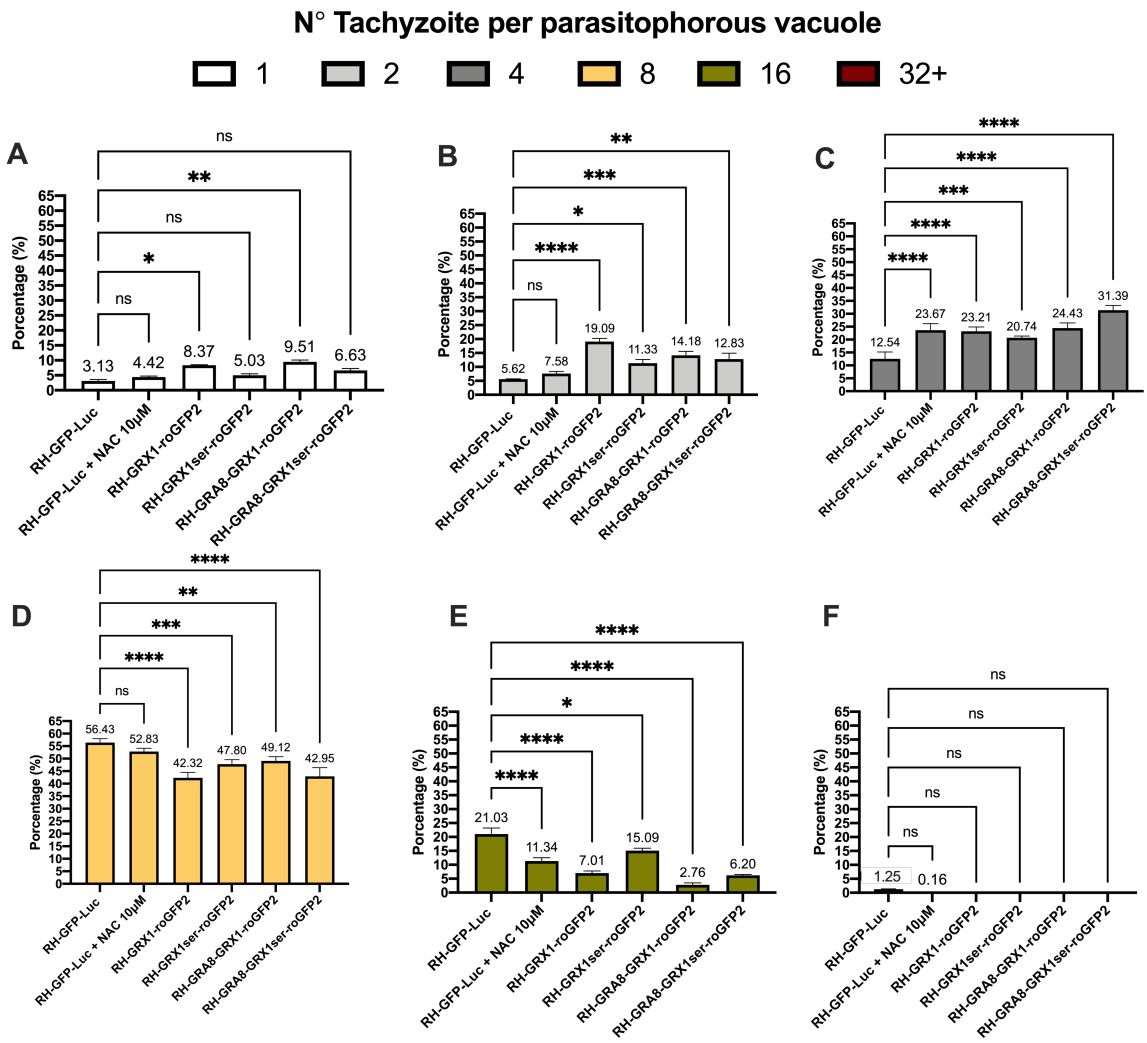

Figure supplement 5: Effect of redox sensors on *T. gondii* parasite growth. Each graph presents parasites/vacuole counts after 20 hours of intracellular growth. The mean values are displayed over each bar for three independent experiments. (**A**) Percentage (%) of vacuoles contain one parasite. (**B**) % of vacuoles with two parasites. (**C**) % of vacuoles with four parasites. (**D**) % of vacuoles with eight parasites. (**E**) % of vacuoles with 16 parasites. (**F**) % of vacuoles with more than 32 parasites. Significance was calculated using two-way Anova, Bonferroni's multiple comparisons test. P values: *< 0.05; **< 0.01, ***< 0.001 and ****< 0.0001.

Primer name	Primer number	Sequence (5'-3')
Fw-GRX1-roGFP2	1	ctcgttggcatttttcttgatggctcaagagtttgtgaac
Rv-GRX1-roGFP2	2	agtgagcacaacggtgattattacttgtacagctcgtccatg
Fw-GRA8-GRX1-roGFP2	3	ctcgttggcatttttcttgatggctttaccattgcgtgttt cggccacggtgttcgtggtcttcgctgtctttggtgtagct cgcgccatggggaaggtggttgtgttc
Fw-GRX1ser23-26	4	ccagcccaccagcccgtacagcag
Rv-GRX1ser23-26	5	atgaacacaaccaccttcccagg
Rv-GRA8-GRX1ser23-26	6	atgaacacaaccaccttccccat
Fw-pTUB8 sequence	7	cagaagacatccaccaaacg
Rv-pTUB8 sequence	8	gctgcgaaacactcctatttag
Fw-jRCaMP1b	9	actttcgtcgtagtcttaatctacttcgctgtcatcatttgtac
Rv-jRCaMP1b	10	tccaggaccaatgctgcagaacgagcttg
Fw-5'UTR of GRA1	11	tgctcaccatcttgcttgatttcttcaaag
Rv-5'UTR of GRA1	12	ccggactacgcgtagttaattcgaaggctgtagtactg
Fw-GFP-t2a-fusion	13	tctgcagcattggtcctggattttcttctacatc
Rv-GFP-t2a-fusion	14	atcaagcaagatggtgagcaagggcgag
Fw-HXGPRT cassette	15	caagaatccccactccaagcatgcaggcgcagctggagaatggcca gaggcaggcatc
Rv-HXGPRT cassette	16	caaccggctgcatgcacgacgaagacatgtgcacctaaagccgcggaa gatccgatcttg
Rv-pSAg1::CAS9-U6::sg1/2 CDPK3	17	aacttgacatccccatttac
Fw-pSag1::Cas9-U6::sg1 CDPK3	18	gacgccagcctcgaaaaggggttttagagctagaaatagc
Fw-pSag1::Cas9-U6::sg2 CDPK3	19	tcagtccgtagttgggacaggttttagagctagaaatagc
Fw-sg1CDPK3	20	gtaatacgactcactatagggcgaattgggtacccaagtaagc agaagcacgct
Rv-sg1CDPK3	21	gtaaaagcttatcgataccgtcgacctcgagaattaaccctc actaaagg
Fw-5'HXGPRT cassette at CDPK3 locus	22	ggagtcacgcctgagtttga
Rv-5'HXGPRT cassette at CDPK3 locus	23	ggcctacgtgacttgctgat
Fw-3'HXGPRT cassette at CDPK3 locus	24	cttcaatgggtttggacgcc
Rv-3'HXGPRT cassette at CDPK3 locus	25	gaacaaagggggtcggtcat
Fw-CDPK3 locus absent check	26	gcgcgttctcaggatgttcgt
Rv-CDPK3 locus absent check	27	cagtgtatctgcaacaaccaga

Table supplement 2: List of primers used to generate plasmid and check sequence / integration in this study.